JTTEE5 8:315-322
©ASM International

Peer Reviewed

Thermal Modeling of Plasma Spray Deposition of Nanostructured Ceramics

I. Ahmed and T.L. Bergman

(Submitted 24 July 1998; in revised form 8 January 1999)

A thermal model for plasma spray deposition of ceramic materials onto metallic substrates has been developed. The enthalpy-based control volume formulation of the heat transfer processes has been used to study the temperature evolution in a two-dimensional substrate and in the coating as it is grown. In this paper, additional melting of ceramic splats after deposition is examined, with a view to predicting the retention of nanostructures in a spray consisting of agglomerated, nanometer-sized particles. Initial results for thin coatings indicate that when the mean temperature of the incoming particles is close to the fusion point of the ceramic material, the nanostructure distribution in the coating is largely determined by the composition of the spray. However, with thicker coatings, additional melting due to prolonged plasma gas heating combined with increased thermal resistance in the underlying coating leads to a loss of nanostructure.

Keywords melting, nanostructured coatings, process modeling, solidification, thermal plasma sprays

1. Introduction

Thermal spray deposition of materials for protection of the substrate against wear, corrosion, and a high temperature environment is a widely practiced industrial process (Ref 1, 2). A recent innovation in this area has been the proposed use of nanostructured ceramic particles, where nanometer-sized particles are reconstituted into micrometer-sized agglomerates suitable for spraying (Ref 3). Among the expected benefits of using such materials is a possible increase in thermal resistance, which makes them attractive for application in the production of thermal barrier coatings (TBCs). An increase in wear resistance and a decrease in machining requirements are also expected.

Spraying nanostructured particles adds a new set of constraints to the already complex array of process control parameters: Overheating can partially or totally melt the agglomerated particles, leading to a partial or total loss in the nanostructure. Conversely, underheating can lead to a decrease in deposition efficiency, leading to high loss rates during spraying as well as poor adhesion characteristics at the coating-substrate interface. Therefore, identifying the optimum operating window is a critical issue.

I. Ahmed and **T.L. Bergman,** University of Connecticut, Contact e-mail: iahmed@engr.uconn.edu.

The purpose of this article is to predict the retention of nanostructure in coatings grown by thermal spray deposition processes. A model is developed that simulates the thermal processes involved in spray deposition. Rather than analyzing the microscopic details of the particle deposition and deformation processes as well as the thermal phenomena evolving inside each of these particles, a global approach is taken where splat-to-substrate as well as splat-to-splat heat transfer is accounted for, while the total combination of substrate and coating is subjected to heating by the spraying plasma (and possibly active cooling on the back side). Similar approaches have been employed in the study of spray forming where molten metal droplets are deposited onto substrates of similar materials (Ref 4). Preliminary results from the present model have been reported elsewhere (Ref 5). For completeness, the key features are summarized in the following paragraphs.

2. The Physical and Numerical Model

2.1 Physical Model

The physical domain of the model consists of a two-dimensional substrate (L_x = 12.5 mm × L_z = 3.18 mm) that has a step change in its thickness at its mid-point (x = 0) to $L_z/2$ (Fig. 1). The substrate is sprayed on its plane side with a moving plasma gun. Substrates of uniform thickness were studied previously in Ref 5, and the variations in temperature distribution were found to be nearly symmetric around x = 0. A nonuniform thickness was chosen in this study to consider the additional thermal ef-

Table 1 Properties of the solid materials used in the simulations

Material	k, W/m · K	c_p, J/kg · K	ρ, kg/m^3	ΔH_f, J/kg	T_f, K	ε
AISI 302	25.4	610	7900	0.26×10^6	1670	0.35
Alumina	7.85	1210	3970	1.07×10^6	2300	…
7YSZ	2.4	620	5700	0.70×10^6	2980	0.25

Data compiled from Ref 13-15

fects on the substrate temperature distribution because it is likely that many objects will have some kind of variation in their thicknesses.

The substrate material was AISI 302 stainless steel with a 30 μm thick alumina bond coating. The material sprayed was yttria (7 wt%) stabilized zirconia (7YSZ). Table 1 provides a summary of the relevant properties of these materials. It should be noted that the thermal conductivity for 7YSZ is the value for the solid form and not for nanostructured agglomerates because accurate data is still not available.

The flight histories of the particles in plasma are not simulated in this work. Rather, the temperature variation of deposited particles and the spatial variation in deposition efficiency are taken into account by using normal (Gaussian) distributions around reference points. All particles are assumed to be of the same size (D_p = 50 μm), and the deposited particles are assumed to impact at the same velocity (V_p = 100 m/s). These assumptions lead to the further idealization that all particles deform equally (the resulting splat size being ≈110 × 5.33 μm, after Ref 6). The kinetic energy (k.e.) of the deposited particle is assumed to be converted to the internal energy of the corresponding splat, that is, $\delta H_{k.e.} = 1/2\rho_p V_p^2$.

Since the possibility of voids forming in the coating is not considered, the splats are modeled to be stacked uniformly in adjacent rows and columns. A constant value of $R_{c,th} = 10^{-5}$ m$^2 \cdot$ K/W is used on all sides of the splats that are in contact with other solid material (Ref 7).

The width of the Gaussian deposition pattern for the splats is specified through a standard deviation of σ_T = 4 mm with respect to the plasma gun axis; the maximum deposition occurs under the gun axis at a rate of Γ = 1 mm/s. These values were chosen to be as realistic as possible upon examination of samples sprayed at an in-house facility.

As mentioned previously, the particle temperatures are assumed to have a Gaussian distribution around a specified mean value. A random variation in particle temperatures is achieved by dividing the total range of the temperature (covering 99% of the population) into 10 K bins and choosing values of temperatures at the center of each bin through the use of a standard random number generator in a Monte Carlo scheme.

The plasma heating characteristics are determined on the basis of empirical results with hot air jets (D_j = 8 mm, V_j = 300 m/s) discharging into a room temperature atmosphere and impinging onto a flat surface (L_{stdf} = 80 mm) (Ref 8, 9), while the plasma gas transport properties are estimated for a mixture of 80% Ar-20% H_2 discharging at T_j = 10,000 K (Ref 10). This configuration leads to the local values of $h_{plas}(x' = 0) \approx 800$ W/m$^2 \cdot$

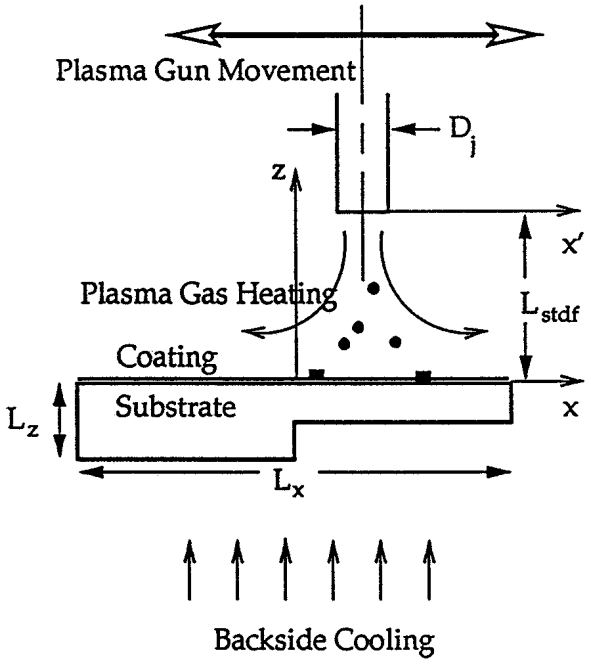

Fig. 1 A schematic representation of the plasma spray coating setup

Nomenclature

c_p	Specific heat, J/kg · K
D	Diameter, mm
f_L	Splat liquid fraction, instantaneous
f_s	Solid fraction, retained (=1 − $f_{L,max}$ at $t \rightarrow \infty$)
h	Local convection coefficient, W/m^2 · K
$\overline{h}$	Average convection coefficient, W/m^2 · K
H	Enthalpy, J/m^3
k	Thermal conductivity, W/m · K
L_{pass}	Spraying gun sweep length per pass, mm
L_{stdf}	Gun to substrate stand-off height, mm (Fig. 1)
L_x	Substrate width, mm (Fig. 1)
L_z	Substrate thickness, mm (Fig. 1)
q''	heat flux across domain boundaries
$R_{c,th}$	Thermal contact resistance, m^2 · K/W
t	Time, s
T	Temperature, K
$\overline{T}$	Mean temperature of incoming particles, K
V	Velocity, mm/s
x	Horizontal coordinate, mm (Fig. 1)
x'	Distance from plasma gun axis, mm (Fig. 1)
z	Vertical coordinate, mm (Fig. 1)

Greek symbols

Γ	Maximum coating growth rate, mm/s
ΔH_f	Heat of fusion, J/kg
ε	Emissivity
θ	Base case coating thickness, ≈283 μm
ρ	Density, kg/m^3
σ_D	Standard deviation in deposition pattern, mm
σ_T	Standard deviation in particle temperature, K

Subscripts

b	Back surface of substrate
c	Coolant
gun	Spraying gun
i	Initial, t = 0
j	Plasma jet, at exit
f	Fusion temperature
p	Sprayed particle
plas	Plasma gas at substrate
s	Deposited splat
surr	Surrounding environment
t	Top surface of coating

K, and $T_{plas}(x' = 0) \approx 5700$ K, respectively, decreasing to $h_{plas} \approx 540$ W/m$^2 \cdot$ K and Tplas ≈ 5400 K at $x' \approx 12$ mm, respectively.

The back of the substrate is assumed to be cooled by natural convection to ambient air, with $\bar{h}_c = 10$ W/m$^2 \cdot$ K and $T_\infty = 300$ K. Radiation exchange between the exposed coating as well as the back of the substrate and the surrounding environment (at $T_{surr} = 300$ K) is also considered. Heat transfer through the edges of the substrate and coating, however, is neglected.

2.2 Numerical Scheme

The numerical algorithm for the prediction of the time-evolving temperature is based on an explicit enthalpy formulation (Ref 11) of the finite volume method (Ref 12). Detailed aspects of the scheme as applicable to the present model can be found in Ref 5. Only a summary is provided here.

In short, the substrate (as well as the bond coating) is divided into discrete control volumes (CV), each of which is assumed to be at a uniform local temperature. Heat transfer between neighboring CV is computed on the basis of Fourier's law of conduction and a linear variation in temperature between the centroids of each CV. The statement of conservation of energy is expressed in terms of the specific enthalpy of the material of the CV concerned:

$$\partial H/\partial t = \nabla \cdot (k_{eff} \nabla T) \qquad \text{(Eq 1)}$$

where H is:

$$H = \begin{cases} \rho c_p (T - T_f) & T < T_f \\ f_L \rho \Delta H_f & T_f < T < T_f + \iota \quad 0 < f_L < 1 \\ \rho \Delta H_f + \rho c_p (T - T_f) & T > T_f + \iota \end{cases} \qquad \text{(Eq 2)}$$

with the reference enthalpy, $H_{ref} = 0$ at $T = T_f$, and $\iota = 10^{-6}$ K. The value of k_{eff} is determined via the values of k and $R_{c,th}$.

In the coating, new CVs (conforming to the shape of the splats) are added as the spraying simulation progressed and the boundary conditions are modified in an appropriate manner. For example, at the top of the coating, heat flux into the exposed splats is $q'' = h_{plas}(T_{plas} - T_t) + \varepsilon_t \sigma (T^4_{surr} - T^4_t)$; the quantities $h_{plas} = h_{plas}(x')$ and $T_{plas} = T_{plas}(x')$ are continuously updated to reflect the lateral movement of the plasma gun. For the back of the substrate, the heat flux out of the domain is $q'' = \bar{h}_c(T_b - T_\infty) + \varepsilon_b \sigma (T^4_b - T^4_{surr})$. All simulations are started with initially uniform temperature in the substrate, $T_i = T_{surr}$.

Since the smallest CVs in the domain of computation represent whole splats, and further discretization of these splats is not attempted, phenomena related to phase changes inside these splats (such as nucleation, solid-liquid front movement, etc.) are not considered. Therefore, the transport of thermal energy is assumed to be dictated by pure conduction (with neighboring splats) and convection (with surrounding gases, for exposed splats). All properties are assumed to be independent of temperature and phase for both splat and substrate materials.

3. Results and Discussion

3.1 Base Case

A base case was run before the effects of the parameters were studied. For all these cases reported in this article, the plasma gun was assumed to be moving parallel to the width of the substrate with $V_{gun} = 250$ mm/s and $L_{pass} = 25$ mm ($=2L_x$), with the center of the sweep coinciding with that of the substrate. The gun was placed to the right of the substrate at the beginning of each simulation.

Sprayed particles were assumed to arrive at $\bar{T} = T_f$ (=2980 K for zirconia) with $6\sigma_T \approx 200$ K. The base case was run for 1 s of spraying time, which amounted to a total of ten back-and-forth sweeps of the plasma gun. The resulting coating, ≈280 μm thick (53 layers of splats), is flat for almost the entire width of the coating, except at the edges. This is the result of a combination of the particular values of the spread in deposition pattern ($\sigma_D \approx L_x/3$), spraying gun sweeping length ($L_{pass} \approx 6\sigma_D$), and gun traversing velocity used in this study.

Figure 2 shows the temperature distribution in the substrate and the coating (the thickness of the latter being magnified by a factor of 10 for clarity) at the end of 1 s. For comparison, a substrate of uniform thickness sprayed under the same conditions has also been included in this figure. The effect of nonuniform substrate thickness shows up in the higher overall temperatures in the thinner section. Temperature variation is also more two dimensional in this section. The thicker section, conversely, acts like a buffer between the high temperature coating on the top and the ambient air at the bottom. A similarity of the temperature variation near the left end of this section to that of the corresponding area of the uniform substrate may be noted.

Temperature distributions in the coatings are relatively more uniform across the width of the coatings, and these distributions are almost identical for both the nonuniform and the uniform substrates. Irregularities evident in the isotherms near the top of the coating indicate recent depositions of hot splats. Higher temperatures toward the right end are a consequence of the location of the spraying gun (the gun is back toward the right end of the sample at the instant of this snap shot) and not as much a result of the nonuniform thickness of the substrate, as observed from similar trends in the coating with a uniform substrate.

Figure 2 also shows the distribution of molten splats in the coating. Here, the light areas mark splats with a retained solid fraction of $f_s \geq 0.99$, where f_s is defined as $1 - f_{L,max}$ at $t \to \infty$ (namely, the maximum solid fraction retained by a splat during the entire period of the spraying process followed by a short period of cooling as tracked at the end of the spraying simulation). Since the normal distribution in temperature was centered around T_f (partially molten particles or particles at exactly T_f but completely in the solid phase was not considered), the number of particles at arrival prior to deposition was equally divided into solid ($f_L = 0$) and liquid ($f_L = 1$) phases. However, no splat that was deposited as a solid was found to have undergone any significant phase change after deposition (the kinetic energy, at $V_p = 100$ m/s, can contribute to a maximum of ≈ 0.7% increment in the f_L of a zirconia splat at T_f). In other words, the ratio of the splats that retained their solid phase during the spraying process to the splats that were completely molten was, for all practical purposes, the same as that of the incoming spray.

Figure 3 presents predicted distribution of the particles in the different incoming temperature bins (as found at the end of the simulation). The slight asymmetry in the Gaussian distribution was due to the particular sequence of the random numbers generated during the course of this simulation.

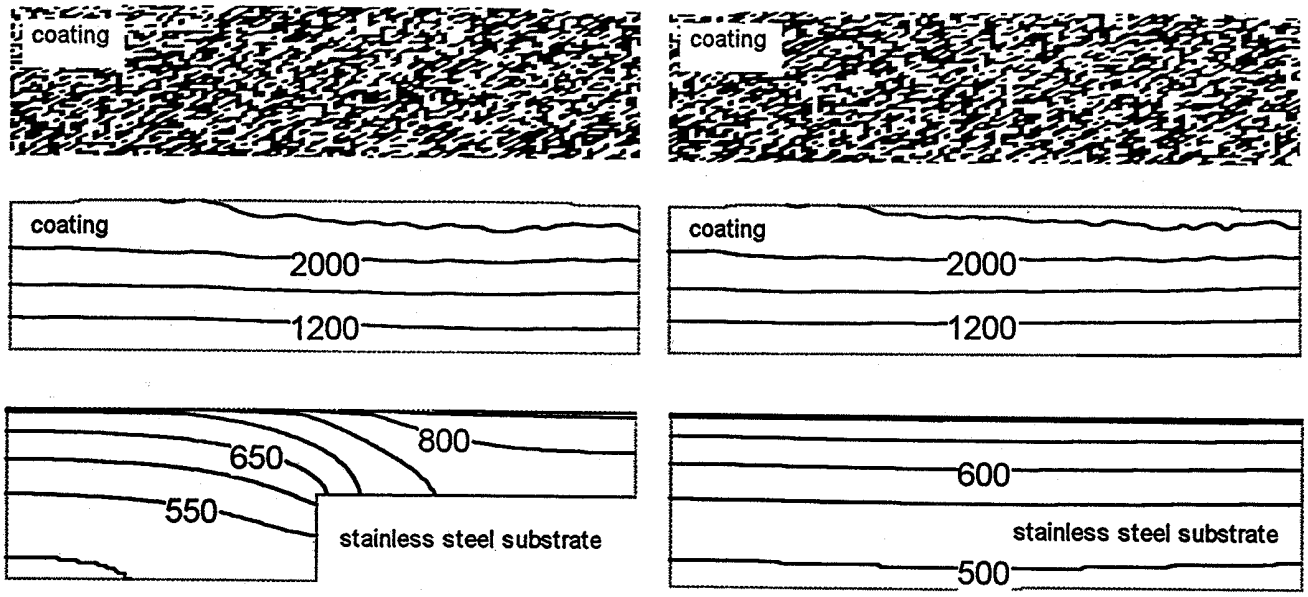

Fig. 2 Predictions for a nonuniform thickness substrate (left column) and a substrate of uniform thickness (right column) at t = 1 s. The top row shows the distribution of splats that retained their solid structure; the dark areas indicate splats that were completely molten. This distribution is similar for the two substrates but not exactly the same because of the statistical randomness in the temperatures of the incoming particles. The contours are lines of uniform temperature: the coatings are shown in the middle row and the substrates in the bottom row. (The vertical axis for the coatings is amplified by a factor of 10).

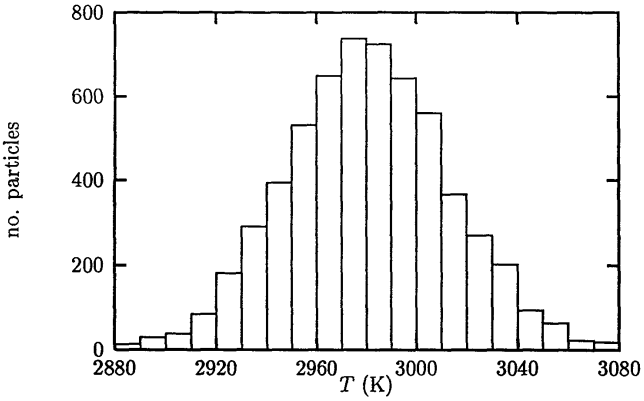

Fig. 3 The temperature distribution of the incoming particles for the base case. Note that although the distribution is always Gaussian in the various simulations, the exact number of particles in each temperature interval varies due to the introduced randomness

3.2 Variation of Standard Deviation in Temperature, σ_T

In order to explore the effect of σ_T of the incoming particles, two sets of predictions were made with similar conditions as in the base case but with $6\sigma_T \approx 20$ K and $6\sigma_T \approx 2000$ K. Figure 4 presents the resulting temperature distributions. The substrate temperatures show no discernible difference. This can be explained by the fact that, overall, the particles carry the same total amount of thermal energy onto the substrate regardless of the value of σ_T. (Some differences must occur because the larger σ_T case will undergo enhanced radiative cooling.) The irregularities in the isotherms of the coating are somewhat amplified for the larger σ_T distribution, obviously because of the larger variation in the temperatures of the freshly deposited splats.

The molten material distributions in the coating for both of these cases were found to be similar to the distribution for the base case, and therefore have not been repeated. Therefore, for these two cases, the f_s distributions in the coating were found to be totally determined by the composition of the incoming spray.

3.3 Variation in Mean Temperature of Incoming Particles, $\overline{T}$

Predictions were made with values of $\overline{T}$ other than T_f. With the same variation as in the base case ($6\sigma_T \approx 200$ K), two sets of results with $\overline{T}$ = 2950 K and $\overline{T}$ = 3010 K, respectively, are shown in Fig. 5. At these mean temperatures, the fraction of molten particles in the spray are approximately 20 and 80%, respectively. The differences in the substrate and coating temperature distributions are explained by the difference in the total energy carried by a respective ensemble of particles in each case. Figure 5 also shows the distributions of molten splats in the coating. The reversed images for the two cases reflect the original composition of the incoming particles. As was revealed upon closer examination, even in the case with $\overline{T}$ = 3010 K, no particle that was deposited in solid form underwent any further phase change for these relatively thin coatings.

3.4 Thick Coatings

In TBC applications, coatings up to 1000 μm can be applied. In order to predict nanostructure retention in plasma sprayed 7YSZ coatings, the preceding simulations were repeated for double the spraying time; that is, 2 s, with all other parameters remaining the same as in the base case. The resulting coatings were ≈560 μm thick.

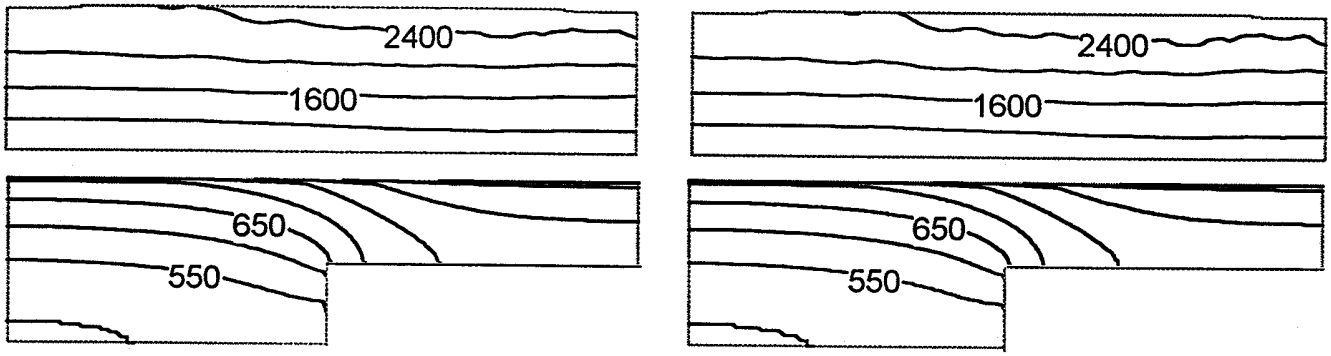

Fig. 4 Predictions with a total temperature spread of the incoming particles, ($\approx 6\sigma_T$) of 20 K (left column) and 2000 K (right column), respectively. The vertical axes for the coatings (top row) have been amplified by a factor 10. The contours are lines of uniform temperature.

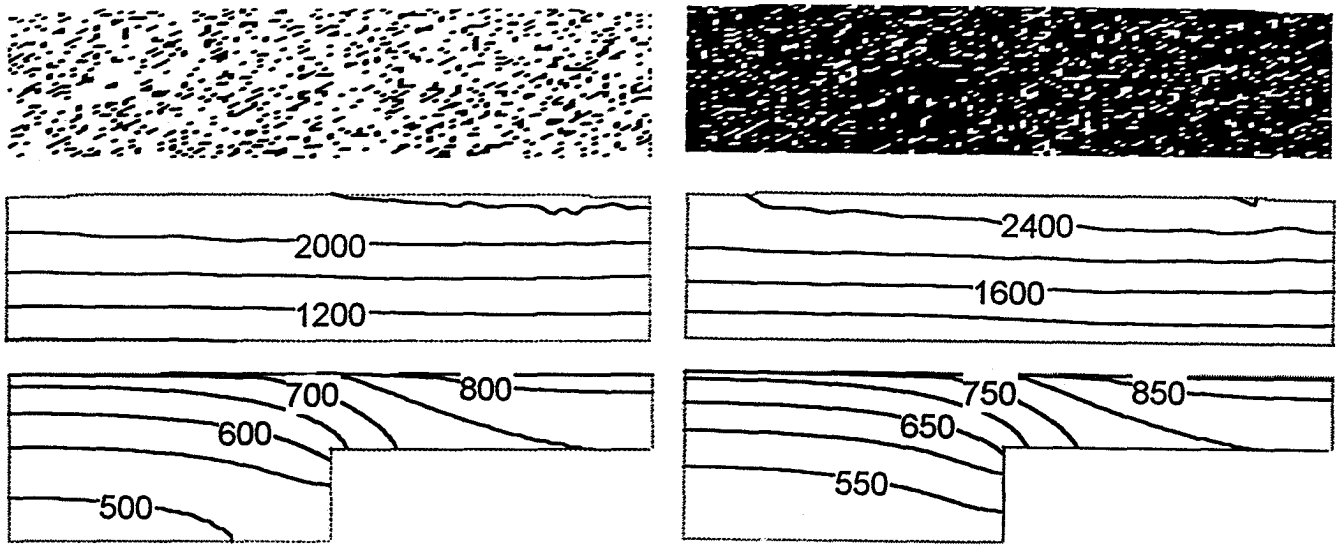

Fig. 5 Predictions with an average temperature for the incoming particles ($\overline{T}$) of 2950 K (left column) and 3010 K (right column), respectively. The top figures show the distribution of splats in the coating that retained their original solid structure (light areas). The contours are lines of uniform temperature.

Figure 6 presents the temperature distributions, as well as the molten splat distribution in the coating. With $\overline{T} = T_f$, the exposed part of the coating began to melt near the end of the process. The slightly higher concentration of molten material near the top (especially toward the right end) indicates that some of the originally solid splats underwent partial or total melting.

Additional melting after deposition can be quantified by plotting a histogram of the number of particles in the different retained solid fraction bins ($\Delta f_s = 0.01$), as presented in Fig. 7. Here fewer splats exist with $f_s \geq 0.99$ than for $f_s \leq 0.01$, because a significant number of splats have lost more than 1% of their solid fraction. In fact, some of the initially solid splats melted completely. Such melting of originally solid splats (and possible remelting of originally molten particles that were solidified after deposition) was primarily caused by the plasma gas heating in conjunction with the increased insulating effect of the coating as the coating thickness increased. Figure 7 shows a distribution of various f_s values along the *z*-coordinate for the entire width of the coating. At $\theta < 1$ (thin coatings; θ being the coating thickness from the base case), no splats are seen at values other than zero or unity (which are not shown in the figure). Partially molten splats appear at larger θ.

Results for thick coatings were also obtained with $\overline{T} = 2950$ K and $\overline{T} = 3010$ K. Figure 8 presents the corresponding temperature distributions as well as f_s distributions. As was seen in Fig. 5, the distribution of the molten splats is reversed for most of the coating in the two cases; however, for the $\overline{T} = 3010$ K case, the completely darkened areas near the top indicate that those splats were completely molten at some time. The temperature contours in the coating (at $t = 2$ s) for the high $\overline{T}$ also show higher (and relatively more uniform) temperature distribution near the top, reflecting the existence of a liquid layer there. Conversely, because of lower overall temperatures, the top of the coating in the $\overline{T} = 2950$ K case was just reaching T_f, and the coating retained nearly all of the solid material composition of the incoming spray. Some partial melting, however, occurred, as shown in the top histogram of Fig. 9. As can be seen, very few splats were molten to $f_s < 0.5$. The histogram for the $\overline{T} = 3010$ K case (Fig.

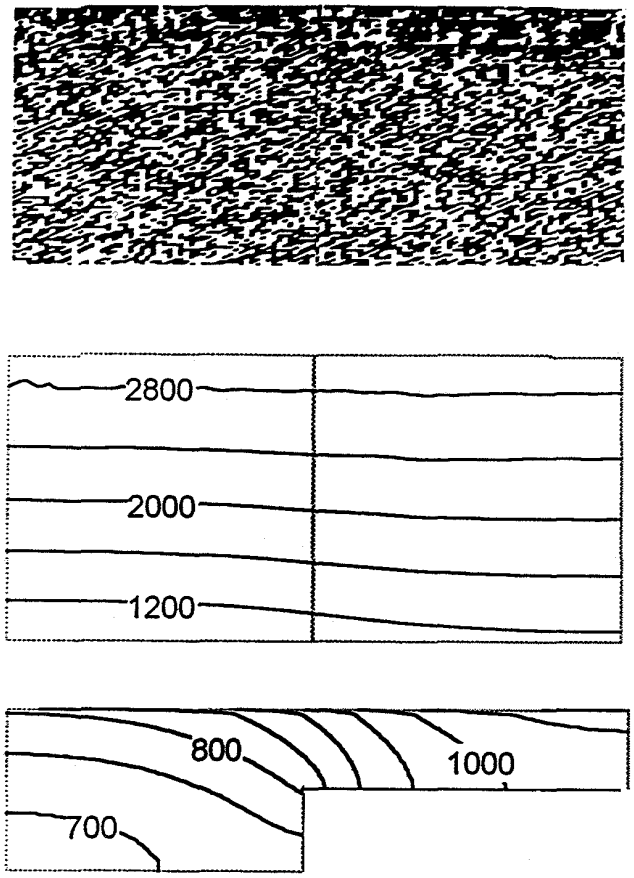

Fig. 6 Predictions for thick coatings (total spraying time, t = 2 s); the top figure shows the distribution of splats that retained their solid structure in the coating (light areas). Additional melting (more dark area) near the top of the coating can be noticed. The vertical axis for the coating is amplified by a factor of 10 as before. The contours are lines of uniform temperature.

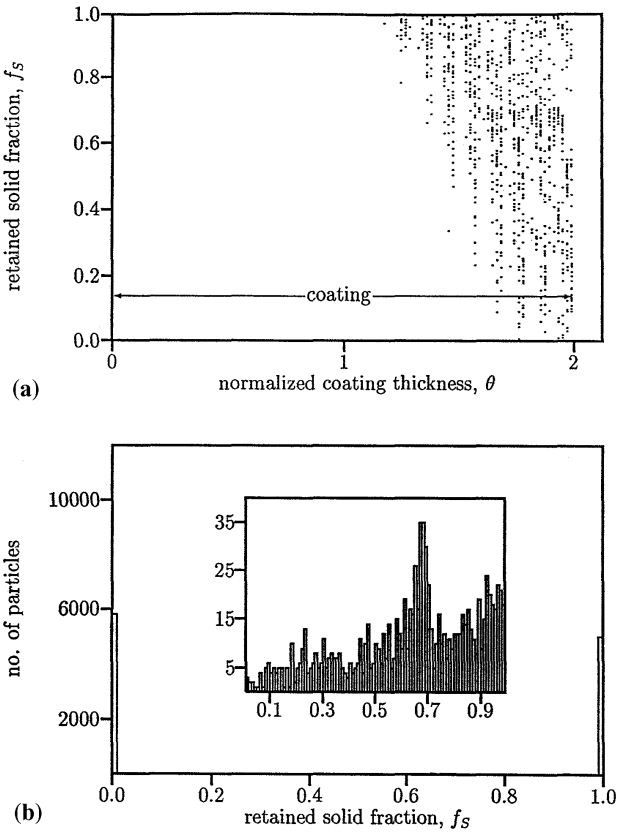

Fig. 7 Distribution of splats with partially retained solid fractions in the thick coating of Fig. 6. (a) The variation in the degree of partial loss of solid fraction through the thickness of the coating ($\theta \equiv$ coating thickness grown in 1 s; total thickness of coating = 2θ); the white region between θ = 0 to $\theta \approx 1$ shows that the splats retained their incoming bipolar distribution of either completely solid or completely molten states through the first second of spraying. (b) Histogram of particles in different retained solid fractions with bin width, Δf_S = 0.01; average temperature, $\overline{T}$ = 2980 K (that is, particles were divided approximately equally between f_L = 0 and f_L = 1 in the incoming spray). The data points between f_S = 0.05 and 0.95 are shown in the inset on an amplified vertical scale.

9, bottom) shows that the distribution of splats throughout the whole range of f_s is more uniform compared to the lower $\overline{T}$ cases. The low population density of splats in the partially molten range can be explained by the fact that a significant number of splats underwent complete melting, as compared to the other two cases.

4. Conclusions

Since partial or total melting of agglomerated nanostructured particles can lead to a dissolution of the nanograin boundaries, the f_s information can be used as a measure of the degree of nanostructure retained in the coating. Based on the predictions, several conclusions can be made:

- The effect of the substrate thickness variation on the coating temperature distribution is minimal.
- The magnitude of the standard deviation in particle temperature, σ_T, does not affect substrate temperature distribution, but increasing σ_T increases the complexity of the temperature distribution in the coating.
- For thin coatings, when $\overline{T}$ is close to T_f, irrespective of the degree of spread in the incoming temperature distribution, the nanostructure retention in the coating is determined by the nanostructure composition of the incoming spray.
- For thicker coatings, a significant loss of nanostructure is possible due to prolonged plasma heating, combined with the enhanced insulating effect.

These predictions exclude the possibility of the development of porosity in the coating. Such porosity will increase the thermal resistance of the coating, thereby promoting melting phenomena for thicker coatings. Also the real temperature distributions for the sprayed particles may not be Gaussian. Finally, the temperature distribution (as well as average values) can depend on the location with respect to the spraying gun axis when particles are injected into the spray in a transverse manner (Ref 16). Both of these factors will influence the predictions.

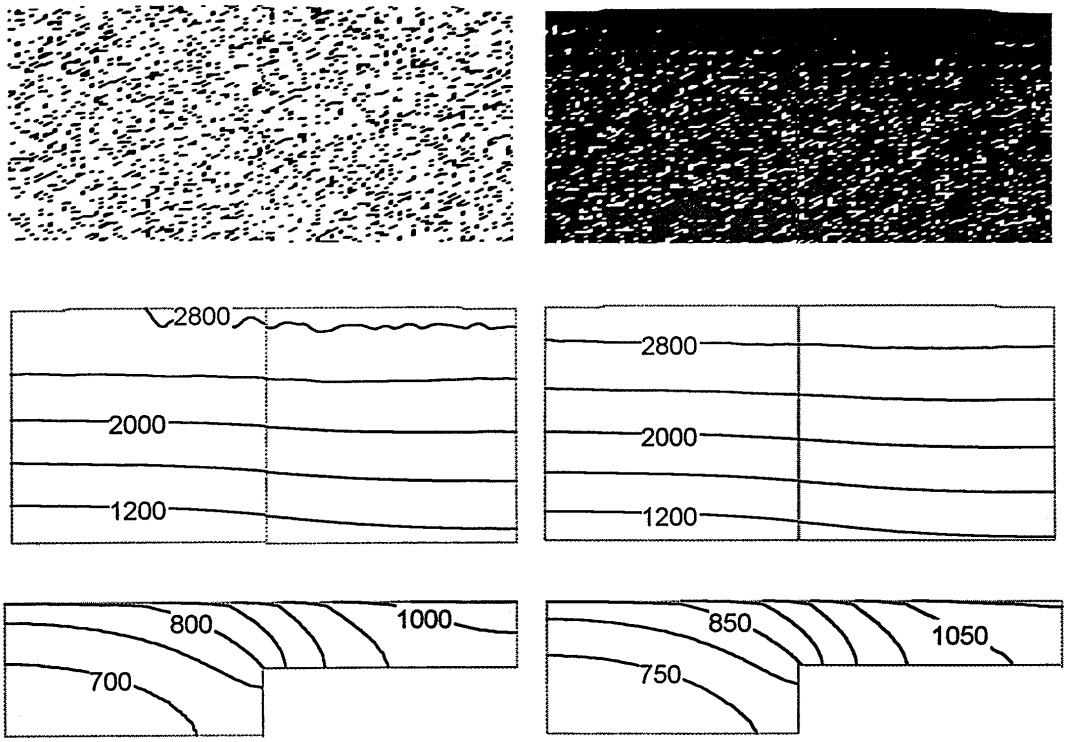

Fig. 8 Predictions for thick coatings grown by spraying for 2 s. Results for an average temperature of the incoming particles, $\overline{T}$ = 2950 K (left column) and 3010 K (right column). The top row shows the distribution of splats that retained their solid structure in the coating (light areas). Additional melting near the top of the high $\overline{T}$ coating is shown in the darker area. The contours are lines of uniform temperature.

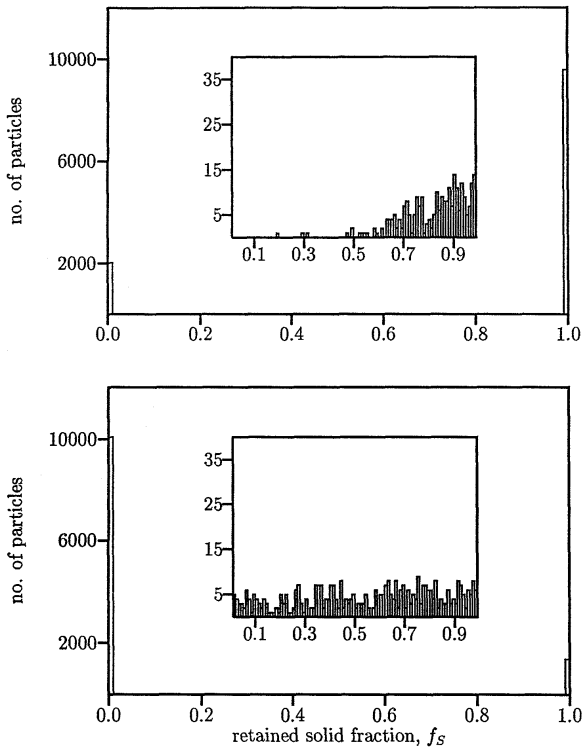

Fig. 9 Histograms for particles at different retained solid fractions with bin width, Δf_S = 0.01; top, $\overline{T}$ = 2950 K (≈20% particles fully molten, f_L = 1, in the incoming spray); bottom, $\overline{T}$ = 3010 K (≈80% particles fully molten in the incoming spray). The insets show the number distribution of particles that underwent partial melting on an amplified vertical scale.

References

1. L. Pawlowski, *The Science and Engineering of Thermal Spray Coatings*, John Wiley & Sons, Inc., 1995
2. D. Poulikakos and J.M. Waldvogel, Heat Transfer and Fluid Dynamics in the Process of Spray Deposition, Advances in Heat Transfer, Vol 28, J.P. Hartnett and Y.I. Cho, Ed., Academic, Boston, 1997, p 1-74
3. M. Gell, The Potential for Nanostructured Materials in Gas Turbine Engines, *Nanostructured Mater.*, Vol 6, 1995, p 997-1000
4. Y. Zhou, Y. Wu, and E.J. Lavernia, Process Modeling in Spray Deposition: A Review, *Int. J. Non-Equilib. Proc.*, Vol 10, 1997, p 95-183
5. I. Ahmed, T.L.. Bergman, and B.M. Cetegen, "A Thermal Model of the Spray Deposition of Ceramic Particles onto a Metallic Substrate," Internal report, The University of Connecticut, 1998
6. G. Montavon, C.C. Berndt, C. Coddet, S. Sampath, and H. Herman, Quality Control of the Intrinsic Deposition Efficiency from the Controls of the Splat Morphologies and Deposit Microstructure, *J. Therm. Spray Tech.*, Vol 6, 1997, p 153-166
7. W. Liu, G.X. Wang, and E.F. Matthys, Thermal Analysis and Measurements for a Molten Metal Drop Impacting on a Substrate: Cooling, Solidification and Heat Transfer Coefficient, *Int. J. Heat Mass Transfer,* Vol 38, 1995, p 1387-1395
8. H. Martin, Heat and Mass Transfer Between Impinging Gas Jets and Solid Surfaces, *Advances in Heat Transfer,* Vol 13, J.P. Hartnett and T.F. Irvine, Jr., Ed., Academic, New York, 1977, p 1-60
9. B.R. Hollworth and S.I. Wilson, Entrainment Effects on Impingement Heat Transfer: Part I—Measurements of Heated Jet Velocity and Temperature Distributions and Recovery Temperatures on Target Surface, *ASME J. Heat Trans.*, Vol 106, 1984, p 797-803
10. B. Pateyron, M.-F. Elchinger, G. Delluc, and P. Fauchais, Thermodynamic and Transport Properties of Ar-H_2 and Ar-He Plasma Gases

Used for Spraying at Atmospheric Pressure. I: Properties of the Mixtures, *Plasma Chem. Plasma Proc.*, Vol 12, 1992, p 421-448

11. J. Crank, *Free and Moving Boundary Problems*, Clarendon Press, Oxford, 1984, p 217-253
12. S.V. Patankar, *Numerical Heat Transfer and Fluid Flow*, Taylor & Francis, 1980
13. W. Krebs, "Multidimensional Radiative Heat Transfer in Gas Turbine Combustion Chamber Wall: Development and Verification from Inverse Calculations," Dr.-Ing. dissertation, University of Karlsruhe, 1995 (in German)
14. D.P.H. Hasselman, L.F. Johnson, L.D. Bensten, R. Syed, H.L. Lee, and M.V. Swain, Thermal Diffusivity and Conductivity of Dense Polycrystalline ZrO_2 Ceramics: A Survey, *Am. Ceram. Soc. Bull.*, Vol 66, 1987, p 799-806
15. F.P. Incropera and D.P. DeWitt, *Fundamentals of Heat and Mass Transfer*, 4th ed., John Wiley & Sons, 1996, Appendix A
16. B.M. Cetegen and W. Yu, In-Situ Particle Temperature, Velocity and Size Measurements in DC Arc Plasma Thermal Sprays, *J. Thermal Spray Tech.*, Vol 8, 1999, p 57-67